Satellite-borne detection of high diurnal amplitude of sea surface temperature in the seas west of the Tsugaru Strait, Japan, during Yamase wind season

by Anindya Wirasatriya

Submission date: 19-Jan-2019 01:16AM (UTC+0700)
Submission ID: 1065745331
File name: 06.pdf (6.09M)
Word count: 9012
Character count: 42976

Journal of Oceanography
https://doi.org/10.1007/s10872-018-0481-1

ORIGINAL ARTICLE

Satellite-borne detection of high diurnal amplitude of sea surface temperature in the seas west of the Tsugaru Strait, Japan, during Yamase wind season

Anindya Wirasatriya[1,2] · Hiroshi Kawamura[3] · Magaly Koch[4] · Muhammad Helmi[1,2]

Received: 12 December 2017 / Revised: 7 May 2018 / Accepted: 26 May 2018

Abstract
The purpose of this study is to investigate the variation of diurnal SST amplitude (ΔSST) in the seas west of the Tsugaru Strait, Japan, which exhibit complex topography that affects the wind pattern during "Yamase" season, when cold easterly winds blow around northeastern Japan. We used infrared based satellite SSTs to obtain strong ΔSST signals. The objective analysis data on surface wind, air temperature and relative humidity patterns was used to explain possible mechanisms responsible for the observed phenomena. Although easterly winds are frequently accompanied by clouds that hinder frequent observation of SSTs from space, four cases of high ΔSST were obtained under clear sky conditions. The results show that high resolution satellite data can capture ΔSSTs of more than 5 °C. Further, the ΔSST variation was strongly influenced by topography. The existence of mountains near the study area have the effect of blocking the easterly winds, creating a low wind speed area on the lee side of the mountain range, which is responsible for the generation of high ΔSST, especially in the offshore area. In addition to the topographic effect, the ΔSST values measured in the in-shore area were influenced by the sea breeze. The warm-dry air mass is advected to the coastal seas by the anti-sea breeze which heats the in-shore area and keeps the ΔSST at the same level as that of the offshore area. This finding highlights the importance of understanding air, sea and land interactions in terms of the variation observed in ΔSST in the study area.

Keywords Diurnal SST · Yamase wind · Topographic effect · Anti-sea breeze · Tsugaru Strait · Infrared SST

1 Introduction

Sea surface temperature (SST) variations have a typical daily temporal scale called diurnal variation of SST which is enhanced by cloud-free conditions and low surface wind (SW) speeds corresponding to the diurnal cycle of air-sea heat flux (Kawai and Wada 2007). In terms of analyzing the air-sea heat flux, the skin SST (hereafter SST_{skin}) should be considered since the atmosphere contacts the sea skin, and not the water at few meters depth. Skin layer is a very thin layer (about 0.1–1 mm) located above the thermocline near the sea surface that develops only during daytime and is referred to as "diurnal thermocline" (e.g., Saunders 1967; Katsaros 1980; Robinson et al. 1984; Ward and Donelan 2006). The temperature at the top of the skin layer is generally several tenths of a degree colder than the temperature below this layer, because eddy diffusion becomes less active than molecular diffusion which occurs close to the surface (Kawai and Wada 2007). Moreover, under clear sky and calm conditions, diurnal thermocline is generated, making the SST_{skin} several degrees higher than the temperature at about a meter below this surface which is referred as SST_{bulk}.

The temperature at the skin layer strongly influences air-sea heat exchange which is a critical component for climate prediction. Webster et al. (1996) found that in the tropical western Pacific, an error of 1 K in SST_{skin} can lead to an error of 27 W m^{-2} in the heat flux estimation. Using hourly

✉ Anindya Wirasatriya
aninosi@yahoo.co.id

1 Department of Oceanography, Fisheries and Marine Science Faculty, Diponegoro University, Jl Prof. Sudarto, SH, Tembalang, Semarang 50275, Indonesia

2 Center for Coastal Rehabilitation and Disaster Mitigation Studies, Diponegoro University, Lab. Terpadu Lt. 1, Jl. Prof. Sudarto SH, Tembalang, Semarang 50275, Indonesia

3 Center for Atmospheric and Oceanic Studies, The Graduate School of Science, Tohoku University, Sendai, Japan

4 Center for Remote Sensing, Boston University, Boston, USA

Published online: 02 June 2018

TOGA Tropical Atmosphere Ocean (TAO) buoys from 1990 to 1996, Zeng and Dickinson (1998) found that, over the equatorial Pacific, the surface latent and sensible heat fluxes showed clear diurnal variability, and the average diurnal amplitudes of latent and sensible heat fluxes were 19.7 and 5.6 W m^{-2}, respectively. That difference is evidently caused by the diurnal cycle in SST_{skin}.

The diurnal SST variation was observed firstly in the 1940s by Sverdrup using SST data gained from vessels (Sverdrup et al. 1942). At that time, the observed amplitude was very small, i.e. <1 K due to the limitation of the data and equipment. These days many researchers have investigated this property using more advanced equipment. For example, by using buoy-observed SSTs, Kawai and Kawamura (2002) developed a regression equation to evaluate the amplitude of diurnal SST (ΔSST) at skin and 1-m depths. The equation uses the daily mean wind speed (U) and the daily peak solar radiation (PS). Their finding reveals some wide patchy areas with ΔSST_{skin} exceeding 3 K and occurring during summer in the tropics and the mid latitudes.

The establishment of satellite measurement in the beginning of the 1980s with high temporal and spatial resolution increased the coverage of ΔSST observations. By using infrared and microwave radiometers, Gentemann et al. (2003) showed the evidence of global diurnal SST variations. A near surface diurnal warm layer is formed during daytime due to solar heating and particularly in regions with low wind speeds. Qin et al. (2007) found that the high ΔSST corresponds to the occurrence of hot events. Hot events are defined as SSTs higher than ~30 °C lasting for a period of more than 10 days and having an areal size of more than 3×10^6 km^2 in the equatorial region as measured from space. Moreover, hourly SST data collected from moored buoys in the western equatorial Pacific also confirm the relationship between hot event occurrence and high ΔSST under clear sky and calm conditions (e.g., Kawamura et al. 2008; Chen and Qin 2016; Wirasatriya et al. 2015, 2016). However, previous studies mainly focused on the ΔSST variation in the global ocean due to the limitation of the spatial resolution of SST datasets (i.e., more than $0.04°\times0.04°$).

In the coastal zone where the land, the sea and the air meet, the mechanism of ΔSST variation becomes more complex. In the present study, the ΔSST variation at seas west of the Tsugaru Strait is studied by using high resolution satellite SST data (i.e., $0.01°\times0.01°$) and high resolution reanalysis wind data (i.e., $<0.1°\times0.1°$). Figure 1a indicates the geographical location of the seas west of the Tsugaru Strait. The seas west of the Tsugaru Strait are part of the northern Japan Sea separating Honshu and Hokkaido Islands. In the Japan Sea, the SST variation is dominated by the annual cycle, i.e., 88–96% of the variations (Nakayama 1951). Thus, researchers mostly focus on the

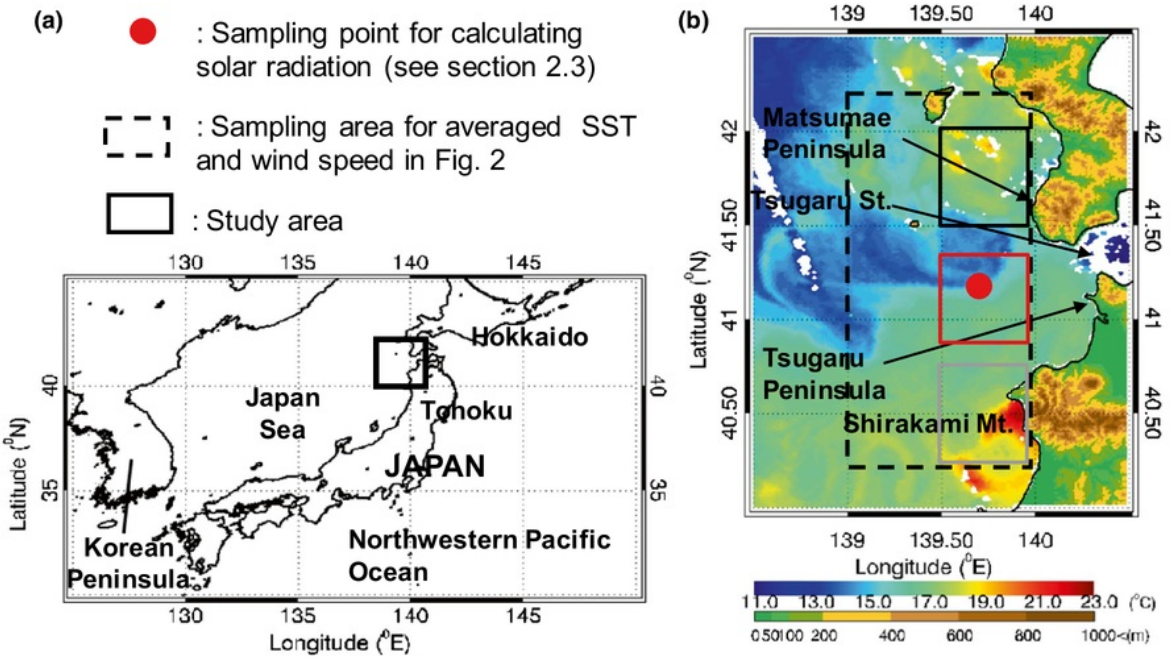

Fig. 1 **a** Geographical location of the study area and **b** its detailed coastlines, land topography and SST on May 24th 2003 at 13.30 JST. Black, red and gray boxes in **b** denote the area for climatological analysis shown in Fig. 3

study of the annual variation of SST in this region. Park et al. (2005) revealed that in the northern region the SST difference between summer and winter can reach approximately 20 °C. Moreover, the greatest north-south SST differences in the Japan Sea occur during winter, i.e., about 16 °C (− 1 to 15 °C). During summer time the difference is only 10 °C (16–26 °C). Large amplitudes of the annual cycle in the northern region of the Japan Sea are related to cooling centers and deep convection sites of bottom-water formation (Kawamura and Wu 1998; Kim et al. 2002; Talley et al. 2003; Park et al. 2005). Beside the annual cycle, semiannual signals of SST variation are also found in the northern region of the Japan Sea with an amplitude of only 2 °C, i.e., about 20% of the annual cycle's amplitude. This is caused by the spatial disparity of SST cooling which generates an asymmetry of seasonal SST variations (Park and Chung 1999; Park and Lee 2014). Thus, no study so far discusses the short-term variation of SST including the ΔSST variation in this region.

One of the forces influencing the short-term variation of SSTs is sea/land breeze. Stull (1988) explained the mechanisms of sea/land breeze. Generally, the land surface has much higher diurnal temperature amplitude variation than the sea surface because the small molecular conductivity and heat capacity in soils prevents the diurnal temperature signal from propagating rapidly away from the surface. As a result, the land is warmer than the ocean surface during daytime and cooler at night. In a constant pressure condition, a temperature increase of matter will be followed by a volume increase which results in a decrease of density. During midmorning (around 10:00 a.m. local time) warm air with less density begins to rise over the warm land near the shoreline, and a denser cooler air from the water flows in to replace it. This is known as the sea breeze. The inland limit of cool air progression over land is known as the sea-breeze front and is marked by low-level convergence (along a narrow band of about 1–2 km wide), temperature drop, and an increase in humidity which is sometimes enhanced by cumulus cloud. A return circulation known as anti-sea-breeze of 1–2 m/s aloft brings the warmer air back to the sea where it descends toward the sea surface to close the circulation. In the absence of a background synoptic flow, the front progresses inland normal to the coastline at speeds of 1–5 m/s. It can easily reach 20–50 km inland by the end of the day. During the presence of opposing synoptic flow, the sea-breeze can stall near the shoreline, or can be totally eliminated as the mean flows from the land to the sea. Conversely, during nighttime the land surface cools down faster than the neighboring water bodies and results in the flowing of cold air from land to sea, and is called the land breeze. The role of SSTs on regulating the dynamics of sea/land breeze has been investigated in many studies (e.g., Sweeney et al. 2014; Franchito et al. 1998). The present study discusses the impact of sea breeze circulation on the generation of ΔSST in the coastal seas near a complex topographic landscape.

Figure 1b shows the complex topographic landscape in the seas west of the Tsugaru Strait with mountains spreading along both sides of the strait. As depicted in the topographic map, the heights of these mountains vary from 200 to 800 m. These topographic variations make low-level routes for the easterly wind from the Pacific to the Japan Sea. The east-west distance of Tsugaru Strait is about 100 km and the width ranges from 20 to 40 km. A previous study by Toyozumi (2004) investigated the SST-surface wind (SW) speed interaction along the west coast of Hokkaido. They found that the generation of high and low SST patterns are related with orographically steered low and high SW in that area. This pattern is shown in Fig. 1. In the summer time during daytime, the areas west of the Shirakami Mountain and Matsumae Peninsula have higher SST than the other areas which may be influenced by the interaction between mountains and the easterly "Yamase" wind. These higher SSTs also may be related to the ΔSST in these areas.

During the period from spring to summer, easterly winds, called "Yamase," dominate in the coastal region of Northern Japan facing the Pacific Ocean. The easterly wind is accompanied by maritime cool and humid air, and low level stratus clouds and fogs that can persist for several days. Since the atmospheric conditions are strongly stable during Yamase season, the surface wind adopts paths over the low-altitude region due to the influence of land topography. This wind blows from a high pressure system over the Okhotsk Sea toward the northern Japan and reaches the Japan Sea through the Tsugaru Strait. It frequently appears in May through August, and sometimes there is continuous blowing for long periods (Yamaguchi and Kawamura 2005; Shimada et al. 2010).

The characteristics of easterly winds in the Tsugaru Strait during Yamase season have been well documented by Shimada et al. (2010) by using satellite-derived SWs. Large-scale and strong local winds are present in the seas west of the Tsugaru Strait and the routes of these low level winds are strongly influenced by topography. Taking advantage of high temporal/spatial resolutions of the satellite SWs, they have pointed out diurnal variations of the surface wind field in/around the Tsugaru Strait.

However, the diurnal variation of SST in seas west of the Tsugaru Strait associated with the wind variations have not been studied yet. Thus, the purpose of this study is to investigate the detailed structure of the diurnal SST variation under easterly winds in seas west of the Tsugaru Strait by using high resolution satellite SST data. Furthermore, the influences of surface wind and land topography are examined in this study, as well as the possible influence of the anti-sea breeze on the occurrence of high ΔSST in the coastal seas. Data and methods are described in Sect. 2. Section 3

describes the relation between ΔSST and wind speed in the seas west of the Tsugaru Strait, and conclusions are given in Sect. 4. Japan Standard Time (JST) is used since this work deals with the diurnal variation.

2 Data and method

2.1 SST data

We used infrared SST image products called the Advanced-HIGHER spatial resolution Sea surface temperature (A-HIGHERS) which have a spatial resolution of 1 km and a temporal resolution of about 2 hours (Sakaida et al. 2000). A-HIGHERS is a product from the Advanced Very High Resolution Radiometer (AVHRR) sensor operated by the National Oceanic and Atmospheric Administration (NOAA) satellites. Because this SST data product is collected by an infrared sensor, it has the advantage that SST is observed only during clear sky conditions which is favorable for the generation of high ΔSST amplitude. The detailed algorithm and cloud detection method of A-HIGHERS is discussed in Sakaida et al. (2000). Furthermore, this SST product also has high accuracy with a bias and root mean square error of 0.02 and 0.51 °C, respectively (Sakaida and Kawamura 1996). The period of observation was from 2000 to 2009.

First, we calculated the monthly climatology mean of ΔSST amplitude in three areas as denoted by small boxes in Fig. 1b, which were selected based on the different topographic effects they may exert on the seas west of the Tsugaru Strait. Black and gray boxes represent the areas in the lee side of the mountain while the red box represents the area in front of the strait mouth. The climatological analysis was performed to show the seasonal variation of ΔSST amplitude in the study area. Following Kawai et al. (2006), we calculated the daily ΔSST amplitude in each box by subtracting the maximum mean SST in the box after 09.00 with the minimum mean SST in the box before 09.00. However, we could not calculate the ΔSST amplitude for the whole days within the period of observation due to the cloud problem. To reduce the calculation error due to the presence of the cloud, we only calculated the daily ΔSST amplitude from the maximum and minimum mean SST if the cloudy pixels in the box were less than 50%. Furthermore, a case study was performed in order to investigate the detailed mechanisms of ΔSST phenomenon in the study area under the easterly wind conditions. We selected about 7600 A-HIGHERS images during the Yamase season (May–August) from 2000 to 2009.

For the selection of A-HIGHERS snapshots, the easterly wind period was defined by using the Sea Level Pressure (SLP) index proposed by Shimada et al. (2010). The Yamase SLP index is the SLP difference between two weather observation stations in the west and east (west–east) side of the Tsugaru Strait. It shows a positive correlation with the zonal component of wind blowing through the Tsugaru Strait. Positive index means that the easterly winds blow and vice versa.

Finally, cloud free day images were selected by visual inspection in order to find strong signals of diurnal SST variation. This step was very important since heavy cloud cover caused by the prevailing winds obstructs measurements of the sea surface SST during this period. In order to obtain a large enough and representative number of cloud-free snapshots, visual screening is the most effective method. Of about 7600 A-HIGHERS images in the study area (black box in Fig. 1b), 91.55% are contaminated with cloudy pixels. Thus, it was very difficult to find a day with clear sky conditions, which are favorable for high ΔSST formation. Moreover, the obtained clear sky images rarely occurred consecutively within a day which is required to represent daytime SST and nighttime SST. Therefore, only in four cases such clear sky conditions were given and thus selected to investigate the characteristic of ΔSST variation in the seas west of the Tsugaru Strait. Each case included 5–9 SST images, which proved that the selected days had almost clear sky conditions and thus signals of the ΔSST variation were significant (Fig. 2). The selected cases showing diurnal SST phenomena occurred on (1) 24 May 2003, (2) 30 May 2005, (3) 8 May 2006 and (4) 4 June 2007.

2.2 Grid-point value data

For investigating the formation mechanisms of high ΔSST, we used the surface atmospheric data from the mesoscale model of grid-point values (GPV). The parameters were surface wind, air temperature (AT) and relative humidity. This dataset is produced by the Japan Meteorological Agency (JMA). The temporal resolution is hourly and spatial resolution is about 10 and 5 km grids before and after 2006, respectively. The GPV data was interpolated using the nearest neighbor method into 1 km to synchronize with the A-HIGHERS resolution.

2.3 Method

Four ΔSST cases were analyzed by producing the ΔSST map, and the averaged wind map. The diurnal SST variation map was produced after visually determining the minimum (min) and the maximum (max) SST images in a day. Since the wind speed has high variability in time, it is very important to consider the period of wind speed that can influence ΔSST variation. Therefore, the acquisition times of the min and max SST scenes were used as a reference to produce averaged wind maps (Fig. 2), assuming that the variation of diurnal SST was determined by the wind speed average

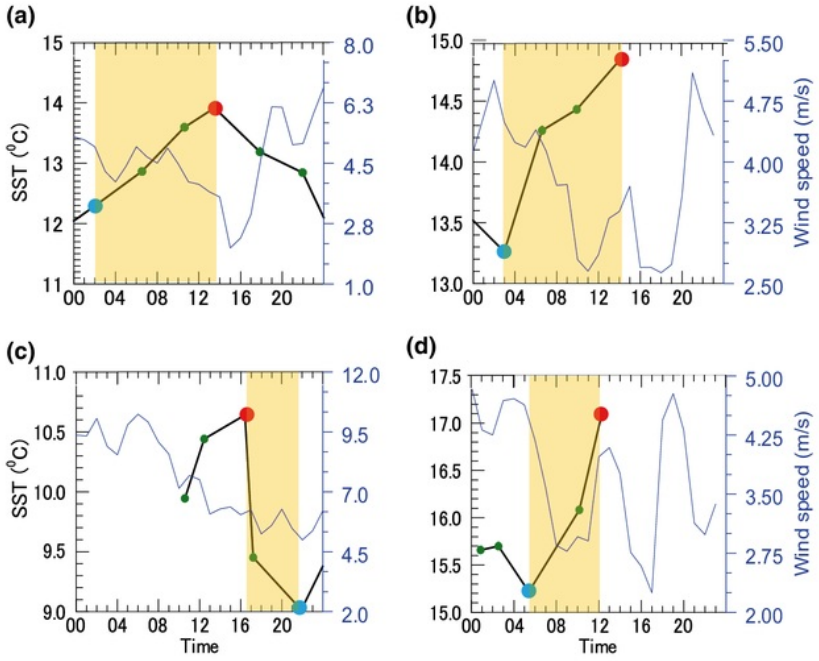

Fig. 2 Acquisition time of max–min SSTs and time series of averaged wind speed in the dashed box indicated in Fig. 1. The *x*-axis is time and the *y*-axis is wind speed (m/s). Green dots connected by thick line denote the acquisition time of A-HIGHERS snapshots. Blue and red dots denote acquisition time of the min and max SST images, respectively. Thin solid line denotes the averaged wind speed variation. The shadowed yellow box denotes the acquisition time of averaged wind speed and min–max SSTs for further analysis in Sect. 3. **a** Case 1: 24 May 2003, **b** Case 3: 30 May 2005, **c** Case 3: 8 May 2006 and **d** Case 4: 04 Jun 2007

Table 1 Regression coefficient for ΔSST model (Eq. 1) from Kawai and Kawamura (2002)

Coefficient	$U > 2.5$ m/s	$U \leq 2.5$ m/s
a	3.0494×10^{-6}	5.0109×10^{-6}
b	-2.8258×10^{-2}	2.2063×10^{-1}
c	-1.1987×10^{-6}	-3.3394×10^{-6}
d	-2.5893×10^{-2}	-2.0216×10^{-1}

between times of the min (blue dots) and the max SSTs (red dots).

For investigating the relation between ΔSST and wind speed for all cases, we used the Kawai and Kawamura (2002) ΔSST model for the skin and bulk SST. The equation is as follows:

$$\Delta\mathrm{SST} = a(\mathrm{PS})^2 + b[\ln(U)] + c(\mathrm{PS})^2[\ln(U)] + d, \quad (1)$$

where ΔSST is the amplitude of Diurnal SST (°C), PS is peak solar radiation (W/m^2) and U is wind speed (m/s). The coefficients of a, b, c and d are listed in Table 1.

For solar radiation data, we approximated by using the short wave radiation formula from Stull (1988) with a cloud-free condition assumption. According to Stull (1988), the intensity of incoming solar radiation at the top of the atmosphere is called solar irradiance (S). The value ranges from 1360 to 1380 W/m^2. Some of this radiation is attenuated by scattering, absorption and reflection from clouds on the way to the earth surface. However in this study, all cases represent clear sky conditions. Therefore, the attenuation due to the cloud was not considered further. The formulae below were used for approximating the solar irradiance intensity at the earth surface in a given area and time, known as downwelling radiation at the surface (Stull 1988).

$$K\downarrow = S \cdot T_{\mathrm{KCF}} \cdot \sin\Psi, \quad (2)$$

$$T_{\mathrm{KCF}} = 0.6 + 0.2\sin\Psi, \quad (3)$$

$$\sin\Psi = \sin\phi\sin\delta_{\mathrm{s}} - \cos\phi\cos\delta_s\cos\left[\left(\frac{\pi t_{\mathrm{UTC}}}{12}\right) - \lambda_{\mathrm{e}}\right], \quad (4)$$

$$\delta_{\mathrm{s}} = \phi_{\mathrm{r}}\cos\left[\frac{2\pi(d - d_{\mathrm{r}})}{d_{\mathrm{y}}}\right], \quad (5)$$

where $K\downarrow$ is radiation at the earth surface (W/m^2), T_{KCS} is transmissivity at the cloud-free condition, Ψ is solar elevation angle, ϕ is latitude (rad), λ_{e} is longitude (rad), T_{UTC} is time (UTC), δ_{s} is solar declination angle, ϕ_{r} is the latitude of the tropic of Cancer (23.45°= 0.409 rad), d is the number of the day of the year, d_{r} is the day of the summer solstice (173) and d_{y} is the average number of days per year (365.25). The position of the sampling point for calculating solar radiation is 139.7°E and 41.2°N and is shown in Fig. 1. Based on the date of each case, the calculated solar radiation for case 1, 2, 3 and 4 were 1006.25, 1014.6, 972.23 and 1019.96 W/m^2, respectively. Since the mean values are close to 1000 W/m^2, we used this value to calculate ΔSST in Eq. (1).

3 Results and discussion

3.1 Seasonal variation of ΔSST in the seas west of the Tsugaru Strait

Seasonal variations of ΔSST amplitudes in the seas west of the Tsugaru Strait are presented in graphical form in Fig. 3. This graph shows overall strong annual signals for the three investigated areas reaching maximum ΔSST amplitudes in the summer time. However, it should be noted that the values of ΔSST amplitudes could have been overestimated, since we neglected the ΔSST amplitudes values during the cloudy days, which should have been very low due to the absence of solar heating. Furthermore, the areas located in the lee side of the mountain had higher ΔSST amplitudes than the area in front of the strait mouth. The annual pattern of ΔSST amplitudes in the seas west of the Tsugaru Strait is very similar to the one found by Kawai et al. (2006) in the Mutsu Bay, which is located only tens of kilometers from the Shirakami Mt., based on buoy measurements. They found that the frequency occurrence of ΔSST amplitudes with more than 1 and 2 °C increased during summer. This is related to the variation of wind speed, which also shows strong annual signal variations, i.e., weakest wind speed in summer. Therefore, in the present study the relation between ΔSST amplitude and wind speed was carefully examined in the case study.

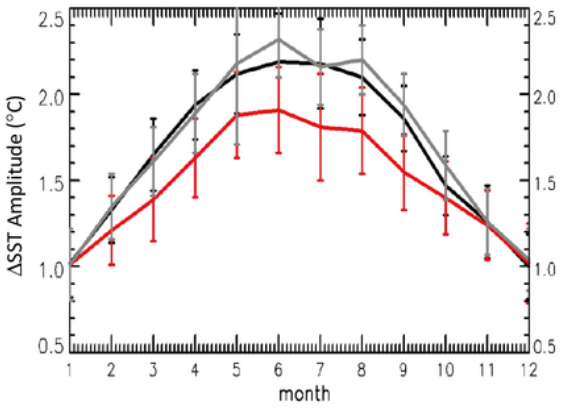

Fig. 3 Monthly climatology mean and standard deviation of ΔSST amplitude in the study area. Black, red and gray lines denote black, red and gray boxes as shown in Fig. 1b

3.2 Spatial analysis of surface wind and ΔSST in the case study area

3.2.1 General condition

In order to describe general features of the four conditions selected for the present study, we present ΔSST and averaged wind vector maps for the ΔSST period (shadowed yellow area in Fig. 2) for each case in Fig. 4. Figure 4 (left) illustrates the averaged wind speed in the seas west of the Tsugaru Strait under easterly wind conditions. Weak wind zones are clearly identified in the seas west of the mountains while strong winds occur in the west of the Tsugaru Strait. However due to the limitation of the GPV data resolution, neither in the Matsumae Peninsula nor in the Tsugaru Peninsula the presence of wind jets in the small gaps between the mountains could be identified as reported by Shimada et al. (2010).

The corresponding ΔSST maps are shown next to the wind vector maps in Fig. 4 (right hand side). Although the detailed features will be described in the following subsections, it should be mentioned here that strong ΔSST signals generally appear in the weak wind areas. Case 3 has the weakest signal of ΔSST due to the very strong wind that occurs in the defined period of diurnal variation. The use of high resolution of SST data allows that a very high ΔSST signal (> 5 °C) can be detected in the area west of the Matsumae Peninsula for cases 1 and 2 and in the lee side of Shirakami Mountain for case 4. This amplitude is much higher than the ΔSST amplitude found by Sverdrup et al. (1942), Kawai and Kawamura (2002), Gentemann et al. (2003), Clayson and Weitlich (2006), Prytherch et al. (2013), Morak-Bozzo et al (2016) in the various locations. This finding is significant, since high ΔSST signals (i.e., > 5 °C) rarely occur even in tropical regions; however, in the present study such signals were detected in a high latitude region during a season when cloudy days are frequent. The use of higher resolution of SST data in the present study may have been the reason for capturing ΔSST values in more detail than previously reported. This assumption is supported by the fact that Kawai et al. (2006) also used A-HIGHERS SST data and found similar high SST signals (greater than 5 °C) in Mutsu Bay. Moreover, they inferred that the satellite SST is more sensitive to the diurnal surface warming than the buoy bulk SST, and reflects skin temperature rather than 1-m-depth temperature. However, they pointed out that the satellite-buoy SST difference does not exactly correspond to the skin-bulk difference, because the satellite SST is originally adjusted to the buoy-observed SST_{bulk}, not SST_{skin}. The bulk-skin SST difference of the observed satellite SSTs is discussed in more detail in Sect. 3.3.

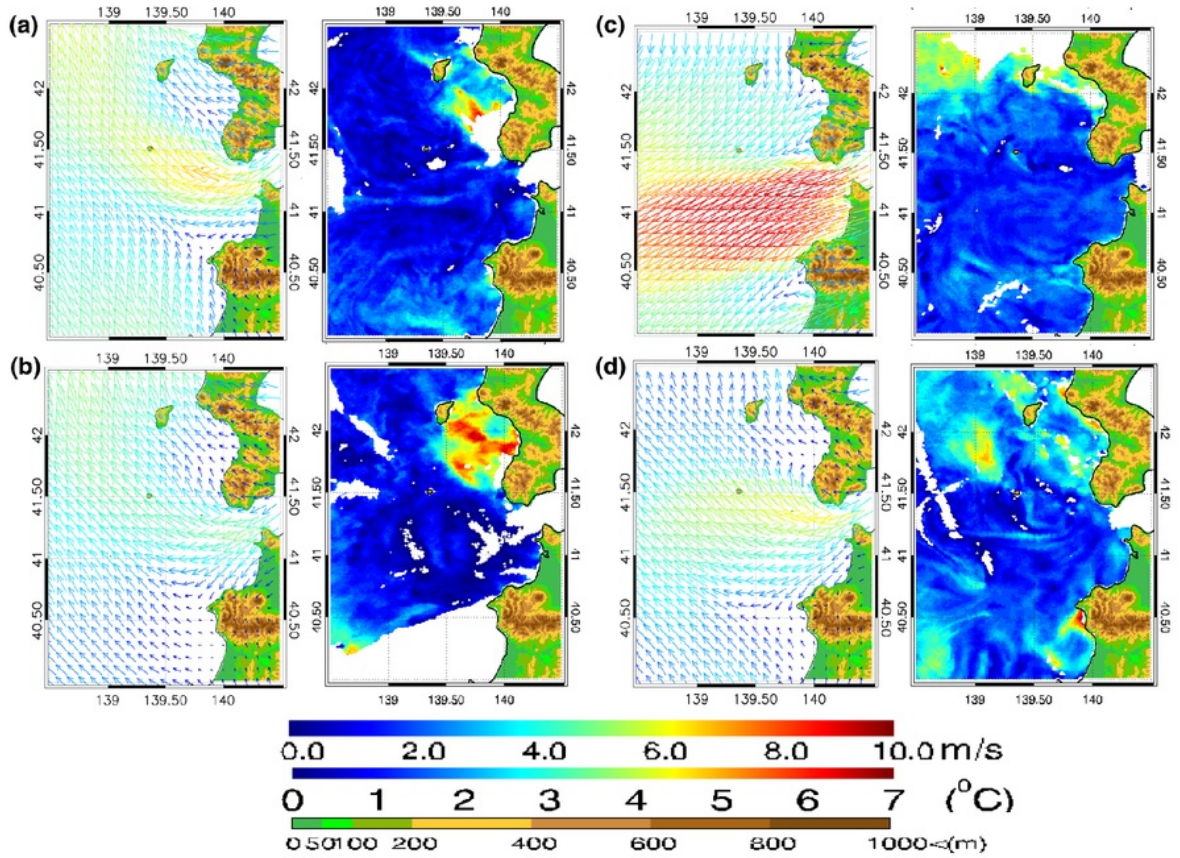

Fig. 4 Averaged wind speed map (left) and ΔSST map (right) of **a** Case 1: 24 May 2003, **b** Case 3: 20 May 2005, **c** Case 3: 8 May 2006 and **d** Case 4: 04 Jun 2007

3.2.2 Case 1: 24 May 2003

A region of strong winds (> 7 m/s) is located in the area of the Strait's mouth (Fig. 4a, left). The low wind areas are identified west of the Matsumae Peninsula and the Shirakami Mountain. The ΔSST signal in the seas west of the Matsumae Peninsula is strong (> 5 °C). This signal is stronger than the one in the sea west of the Shirakami Mountain (Fig. 4a, right).

3.2.3 Case 2: 30 May 2005

The wind speed in case 2 is the lowest among the selected cases. The maximum speed in the mouth area of the Strait is only 5 m/s (Fig. 4b, left). This condition forms the wide weak wind area in the lee side of Matsumae Peninsula, where the strongest signal of ΔSST occurs. From Fig. 4b (right) the strong ΔSST signal (> 5 °C) covers more than the 1°× 1° area of west of the Matsumae Peninsula (Fig. 4b, right). However, due to the cloud cover, the ΔSST signal in the lee side of the Shirakami Mountain could not be observed.

3.2.4 Case 3: 08 May 2006

Case 3 is characterized by very strong winds flowing out of the Strait (Fig. 4c, left); and around the area of the strait mouth, the wind speed reaches about 10 m/s. However, the high topography still plays a significant role in creating weak wind areas in its lee sides. Because of the influence of very strong easterly winds, ΔSST signal is not so large in case 3 (Fig. 4c, right). In the lee side of the Shirakami Mountain, the ΔSST amplitude is less than 3°C, and higher ΔSST signals are seen in the narrow band along the lee side of the Matsumae Peninsula.

3.2.5 Case 4: 04 Jun 2007

The high wind speed at and around the strait mouth is almost the same as that of case 1. The averaged wind speed is about

6 m/s (Fig. 4d, left). The areas of low averaged wind speed are identified in the lee sides of the Matsumae Peninsula and the Shirakami Mountain as a result of a topographic effect.

Strong ΔSST signals appear in the coastal seas west of the Shirakami Mountain though the located signal area is small. A wider area of ΔSSTs with smaller amplitudes is found in the lee side of the Matsumae Peninsula (Fig. 4d, right). Thus, all cases demonstrate that high ΔSSTs were found in the lee side of mountains.

3.3 Relation between ΔSST and wind speed

By considering the observational evidence of ΔSSTs in the four cases of clear-sky and easterly wind conditions and the relation between ΔSST and wind speed as described by Kawai and Wada (2007), the study area was divided into three areas A, B and C as shown in Fig. 5a. Area A and C are characterized by low wind speeds and high ΔSST amplitudes while area B shows high wind speeds and low ΔSST amplitudes. In the present study, the sea area west of 139.2°E was not studied further because of the occurrence of high DSST signals, and it was found not to be affected by topography as in the coastal areas of A, B, C, and thus was considered not relevant for this study.

In order to analyze the relation between the observed ΔSST phenomenon and wind speed quantitatively, we sampled the ΔSST signals. Since each case and area had a different pattern/shape of the ΔSST signal, we adopted a circular sampling shape with 20 km in diameter for parameter sampling. The usage of a 20 km diameter circle was based on visual observation of the ΔSST images in Fig. 4. The visually selected circles are indicated in Fig. 5 for each case. Within the 20 km circles, 0.01° gridded ΔSST and wind speed were sampled and statistically analyzed. With the exception of the grids overlaid by the circle lines and clouds, the average number of available grids in one circle is about 300. In order to avoid sampling errors and biases, we used as a sampling criterion a standard deviation threshold of ΔSST < 1.0 °C.

Histograms of the mean ΔSSTs and their standard deviations are presented in Fig. 6. Figure 6a shows that area A has mean ΔSST amplitudes ranging from 0–5 °C while area B has ranges from 0–1 °C. The mean amplitude of area C is in the middle. Since the mean ΔSST amplitude in area B is almost uniform, their standard deviation is less than 0.4 °C (Fig. 6b). In contrast, the standard deviations of areas A and C are distributed in the range of 0–1.0 °C. Because of the quality check threshold, all the standard deviations are smaller than 1.0 °C.

Figure 7 shows the relations between the circle-averaged ΔSST and wind speed. The compilation of all cases shows that the ΔSST decreases with increasing wind speed following logarithmic pattern. The correlation coefficient is −0.55. Under clear and weak wind conditions, solar radiation heats the sea surface effectively, forming the thermocline near the surface (diurnal thermocline) which increases ΔSST. Because of the conditions set for selection of SST images in the present study, the clear-sky condition is automatically satisfied.

The topographic effects on easterly winds are responsible for generating low (high) wind speed areas in the lee side of the mountain (in the strait mouth), which are geographically fixed. The existence of mountains acts as a barrier blocking the easterly winds. On the other hand, the existence of the strait may act as a wind corridor producing the expansion fan mechanisms described by Shimada et al. (2010), and bursting the wind jet off the strait mouth. Furthermore, the decrease of wind speed in the lee side of the mountain may reduce the latent heat release which increases the warming effectiveness under clear sky conditions (e.g., Qin et al. 2007; Wirasatriya et al. 2015). In terms of an oceanic process, Wirasatriya et al. (2017) explained the role of wind speed in the mechanical mixing occurring in the water column, which controls the heat transport from the surface to the deeper layer. The reduced wind speed may damp the mechanical mixing, allowing the formation of a near surface thermocline and subsequent generation of high ΔSST. However, these possible mechanisms still need to be examined further by using heat flux data and subsurface oceanic data, and require future studies.

A comparison of the observed and modeled ΔSST is presented in Fig. 7. Although the A-HIGHERS SST algorithm is tuned against the SST_{bulk} (Sakaida et al. 2000), which may differ from the SST_{skin}, the models proposed for the 1 m depth SST (SST_{bulk}) do not present a strong relation between ΔSST and wind-speed. In this figure we can clearly observe that the pattern of the observed ΔSST agrees better with the model ΔSST for SST_{skin} than SST_{bulk}. The bulk model underestimates the ΔSST especially for wind speeds that are less than 2.5 m/s. The distribution of observed ΔSST follows the logarithmic pattern of the skin model.

The skin model of Kawai and Kawamura (2002) works better than their bulk models in describing the relation between wind speed and ΔSST in the seas west of the Tsugaru Strait. Kawamura et al. (2008) have investigated the bulk-skin SST problem in terms of the satellite SST observation for a hot event case. A hot event is a high SST phenomena of about or more than 30 °C which is characterized by the large ΔSST and occurs under clear sky and weak wind conditions. Kawamura et al. (2008) have shown that the satellite SSTs have a systematic positive bias against the corresponding buoy SSTs in a HE region. The bias is enhanced in conditions of large in-situ ΔSST. One-dimensional numerical simulation of the SST and the near-surface thermal structure suggests that the systematic bias between the satellite- and buoy-measured SSTs may be caused by

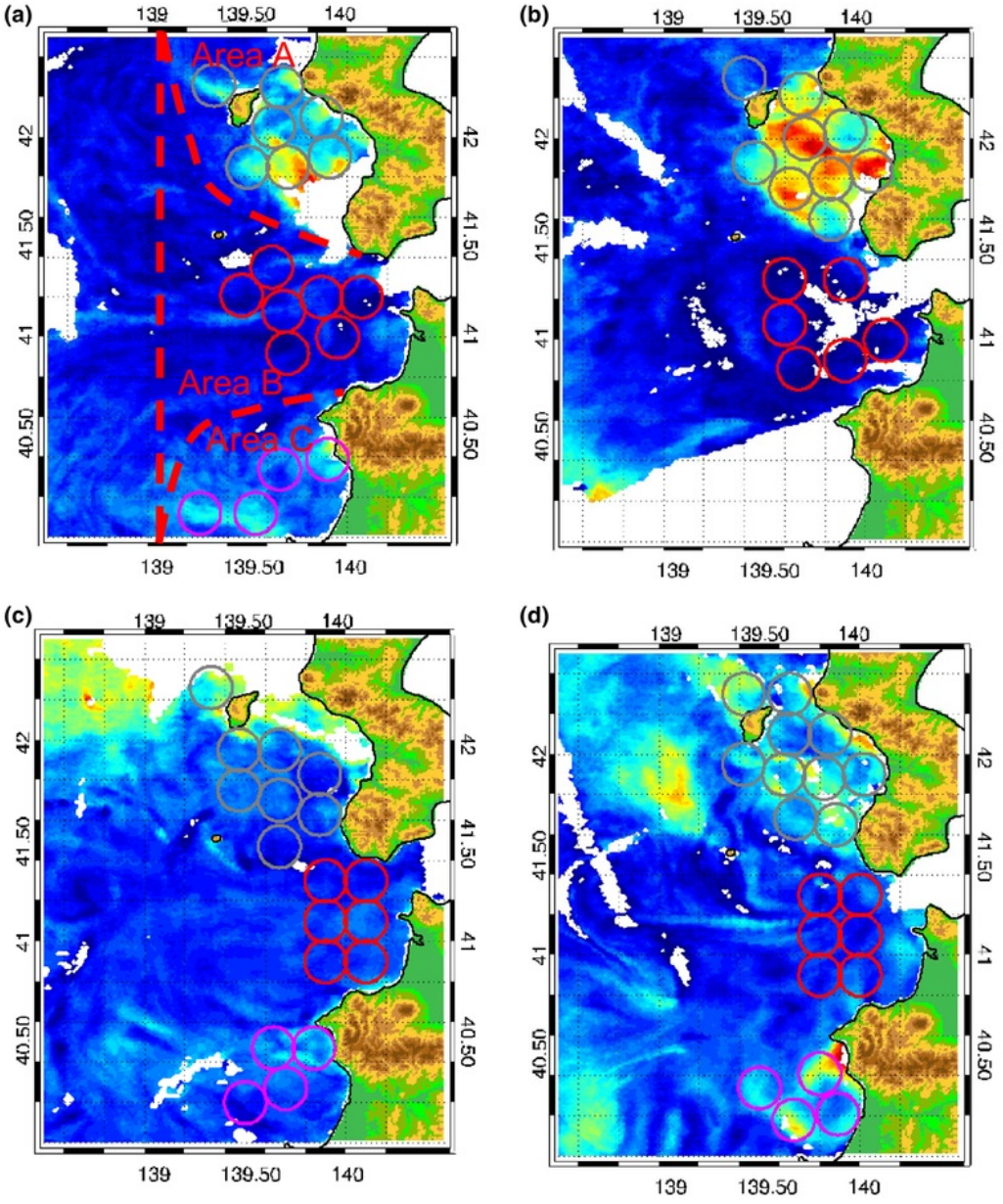

Fig. 5 The position of circle samples. Grey, red and purple circles are samples for Areas 1, 2 and 3, respectively. **a** Case 1: 24 May 2003, **b** Case 2: 30 May 2005, **c** Case 3: 08 May 2006, and **d** Case 4: 04 Jun 2007

the regularly formed, sharp, vertical temperature gradient in the surface layer of a HE region. The widely used satellite SST algorithm is statistically tuned against the globally distributed in situ buoy SSTs. It is reasonably considered that the buoy SSTs are equivalent to the surface SST_{skin} in a statistical sense because of random temporal/spatial match-up sampling for comparison with the satellite SSTs. However, during clear sky and weak wind conditions which enhance the increase of SST and establish the thin warm layer, the satellite SSTs derived from the global algorithm may estimate bias against the SST_{bulk} from buoys. Thus, during the high ΔSSTs occurrences, A-HIGHERS SSTs sensed the SST_{skin} which was higher than the SST_{bulk} and induced the positive bias in the buoy's validation. According to this

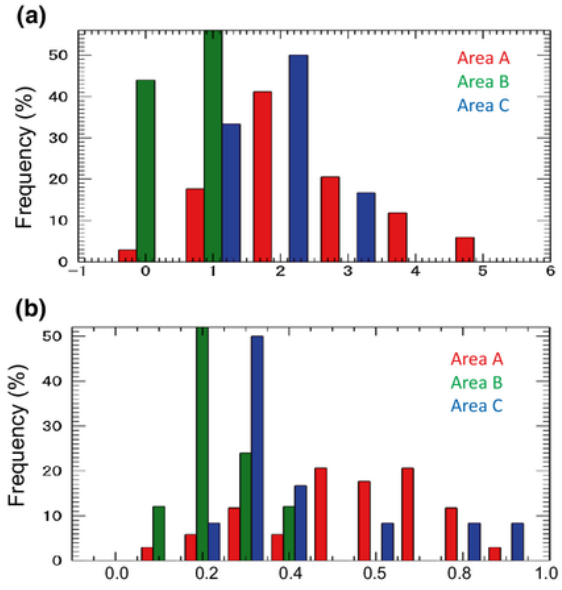

Fig. 6 Histograms of **a** mean ΔSST and **b** standard deviation for all samples shown in Fig. 4

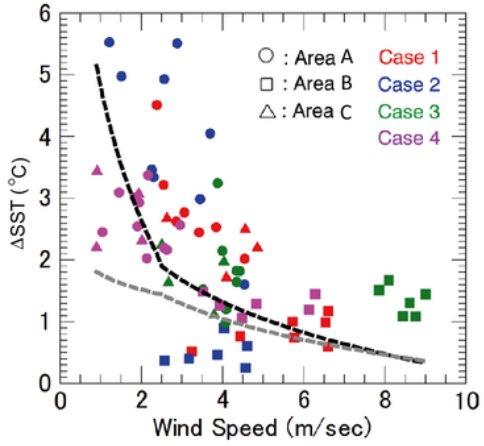

Fig. 7 Relations between ΔSST vs wind speed for all samples shown in Fig. 5. The dashed black (gray) line is the skin (bulk) ΔSST model generated from Eq. (1)

reasoning, the skin model is better to express the relation between wind speed and ΔSST than the bulk model.

3.4 Possible effect of sea breeze

Sea/land breeze is a common air-sea-land phenomenon that occurs in the coastal zone. During daytime, sea breeze blows from the sea to the land which has the effect of cooling SSTs. However, the present study indicates that the high ΔSST is maintained along with the possible cooling effect of the sea breeze. In this section the contribution of sea breeze on ΔSST generation in the coastal area is investigated together with its interaction with high topography and synoptic wind background, i.e., easterly wind.

We chose the case with the highest ΔSST among all cases for this analysis, i.e., area A of case 2. In Fig. 7, the ΔSST in area A case 2 (the blue circles) are greater than 4°C. Figure 8 indicates the GPV time series of (a) surface wind speed, (b) surface wind direction, (c) air-temperature and (d) relative humidity in the numbered sampling circles for area A of case 2. In Fig. 8a, we divided the circles into three categories, i.e., the in-shore circles (no. 5, 7, and 8), the middle-distance circles (no. 1, 2 and 6) and the offshore circles (no. 3 and 4). The temporal variations of wind speed and direction are shown in Fig. 8b, c. During nighttime, the wind direction is north-westward, leaving from the coast. The wind speed in the coastal circles is higher than that in the offshore circles, which may be attributed to the land breeze. Its existence is also enhanced by the easterly wind of a synoptic flow field.

In the morning, when the land surface is heated, the wind speed decreases following the direction of change from north-westward to eastward especially in the in-shore circles. The minima of decreased wind speeds are recorded at around 10:00 a.m. The wind speed increases in the afternoon (i.e., 14:00) toward the land in the in-shore circles. These changes of wind fields are consistent with developments of the sea breeze. Moreover, the GPV AT map at 14:00 (Fig. 9a) also demonstrate that the AT over the land is much higher than the seas which is favorable for inducing sea breeze generation. Nevertheless, the existence of opposing synoptic flow of an easterly wind as illustrated in Fig. 4b causes the sea breeze to be influenced by the background wind field, i.e., easterly wind. In this case, the high topography in the Matsumae Peninsula plays an important role to block and reduce the strength of the easterly wind.

The impact of the sea breeze on the surface layer is the anti-sea breeze in the upper atmosphere layer. Indications of anti-sea breeze occurrence are evidenced by the time series of AT (Fig. 8d) and relative humidity (Fig. 8e). The AT in the in-shore circles increases rapidly during daytime whereas relative humidity shows the reverse. This may be caused by the anti-sea breeze blowing from land and carrying a warm and dry air mass toward the coastal sea. However, since we did not use the atmospheric data in the upper layers (we only used the parameters of the surface layer), the appearance of anti-sea breeze is not described in the vertical section. This problem needs to have further investigation in the future.

The role of anti-sea breeze on the generation of high ΔSST near the coastline is also shown in the AT–SST difference map during the time of maximum SSTs (Fig. 9b). The negative difference in the offshore area indicates that AT is lower than SST. Thus, the increasing SST in the offshore

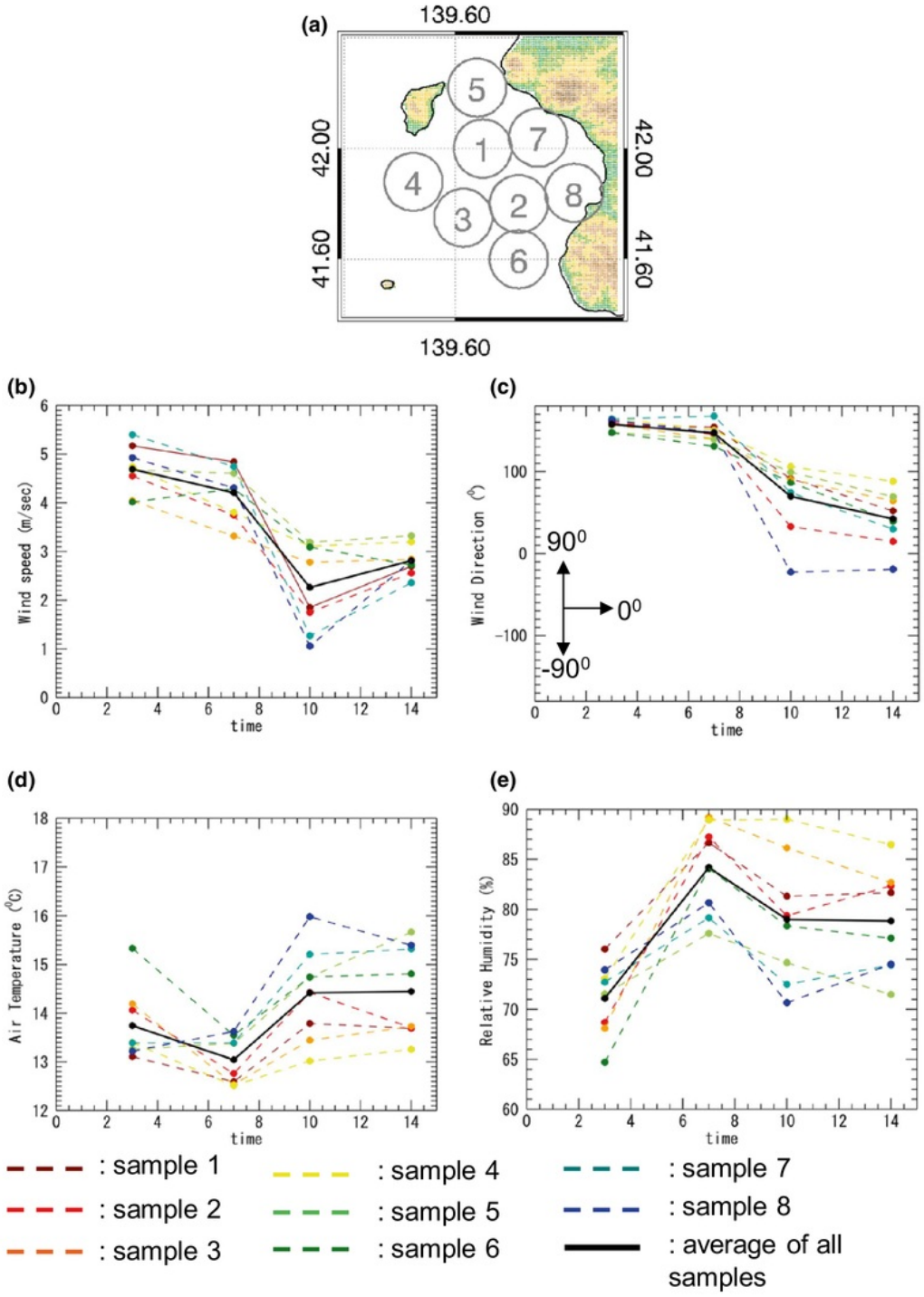

Fig. 8 Time series variation of wind speed, wind direction, air temperature and relative humidity in area A of case 2: 30 May 2005. **a** The location of numbered circles, **b** wind speed, **c** wind direction, **d** air temperature, and **e** relative humidity

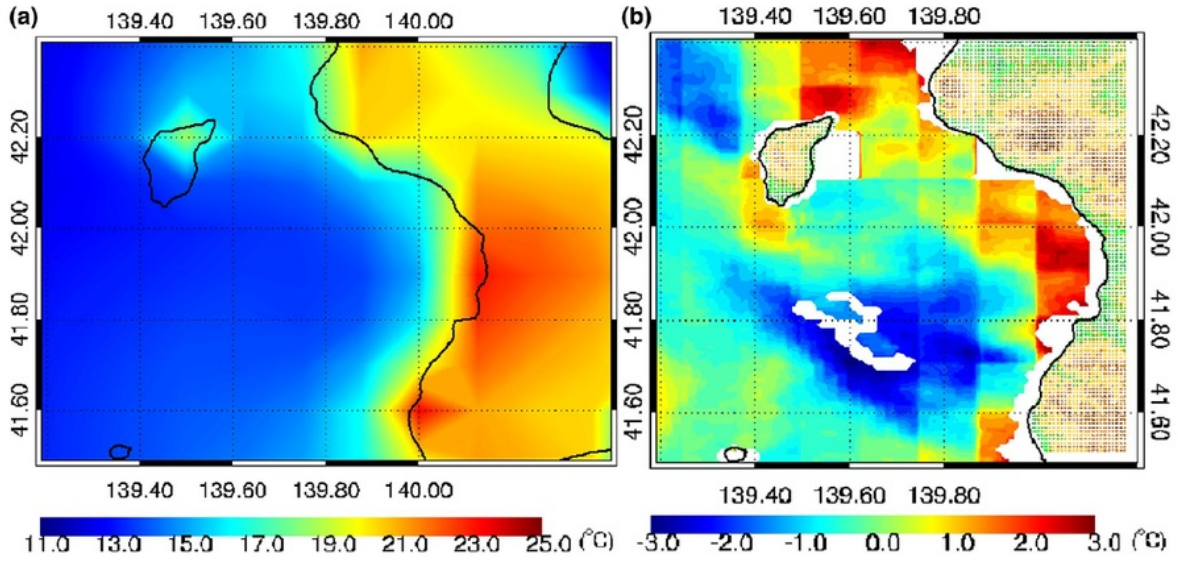

Fig. 9 **a** Air temperature map on 30 May 2005, time: 14.00. **b** Difference map of air temperature–SST for area A of case 2: 30 May 2005, time: 14.00

area during day time corresponds to the clear sky and calm condition which eventually enhances the ΔSST. In contrast, the positive difference along the coastline means that AT is higher than SST. This indicates that the temperature of down-welling air mass caused by the anti-sea breeze was much warmer than the SST. Consequently, the sea surface was heated as the effect of the heat gain from sensible heat flux in the seas along the coastline. This process may contribute to the enhanced ΔSST in area A of case 2. However, at the same time, the warm-dry air mass over the sea surface enhanced the heat exchange due to the latent heat flux (i.e., the sea loses heat). Hence, this warm and dry air mass heated and cooled the coastal seas and kept the ΔSST at the same level as that of the offshore areas.

The influence of anti-sea breeze only happened in a narrow area. Figure 8b also shows that the positive difference only occurs along the coastline with the width of the band about 10–20 km from the coastline. This distance is called the horizontal distance of sea breeze circulation. This distance is consistent with the in situ observations (e.g., Stull 1988; Asai 1996) and the linear theory of sea breeze (e.g., Niino 1987). Many studies have investigated the role of SST in the coastal seas on the dynamics of sea breeze (e.g., Sweeney et al. 2014; Franchito et al. 1998). Moreover, Kawai et al. (2006) suggested the role of diurnal warming of SST on reducing the local atmospheric circulation related to the sea breeze in Mutsu Bay. The weakening of that circulation is caused by the decrease of the land-sea temperature difference as a result of the increasing SST during daytime. Thus, considering the whole results, the present study emphasizes another point of view of the relation between ΔSST variation and sea breeze circulation, i.e., the generation of high ΔSST in the coastal area is influenced by the sea breeze.

4 Summary

We visually investigated diurnal SST amplitude in the seas west of Tsugaru Strait by using SST products derived from satellite SSTs obtained from high resolution infrared sensors. Although during the Yamase season (May–August) from 2000 to 2009 the occurrence of an easterly wind was often accompanied by cloudy conditions, we managed to collect four cases with strong ΔSST signal under the conditions of clear sky for investigating the characteristics of ΔSST phenomenon in the seas west of Tsugaru Strait.

High ΔSST amplitudes (i.e., > 5 °C) are identified in the lee side of the mountains in the Matsumae Peninsula and in the Tsugaru Peninsula (the Shirakami Mountains), while low ΔSST amplitude (i.e. < 1 °C) are obtained in the west of the strait mouth. Thus, it can be concluded that the ΔSST variation in the seas west of the Tsugaru Strait is strongly influenced by land topography. In the lee side of the mountain where the wind speed is low, the amplitude of ΔSST is high.

Figure 10 summarizes two possible warming mechanisms that lead to the very high ΔSST phenomenon (i.e., > 5 °C) in the sea west of Matsumae Peninsula on 30 May 2005 (Case 2). The first mechanism is the shortwave radiation heating under clear sky and calm conditions which becomes the main warming mechanism (Fig. 10a). The easterly wind

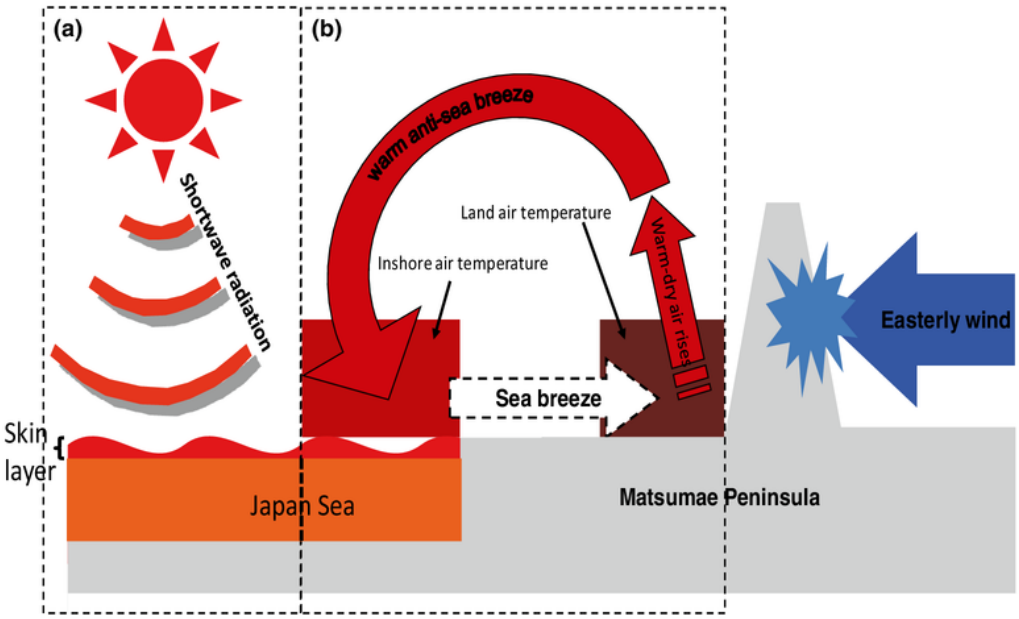

Fig. 10 Warming mechanism over area A of case 2: 30 May 2005. **a** Offshore warming due to high solar radiation under a weak wind condition. **b** Coastal processes induced by warm anti-sea breeze blowing from land toward coastal sea surface. The darker red means the higher air and sea temperatures

blowing in this case was the weakest among the selected four cases. Easterly winds were blocked by the high topography of the Matsumae Peninsula, creating a wide weak wind area in its lee side. As stated in Qin et al. (2007) and Wirasatriya et al. (2015), weak wind conditions reduced latent heat release so that SST could be effectively warmed by solar radiation during daytime and increased the ΔSST. Along the coastline, a zone with a width of about 10–20 km shows high ΔSSTs that are influenced by the sea breeze; along this zone the warm-dry air mass is advected by the anti-sea breeze (Fig. 10b). This warm and dry air mass heats/cools the coastal seas and keeps the ΔSSTs at the same levels as that of the offshore area.

Acknowledgements We gratefully thank the support from the Ministry of Research, Technology and Higher Education (KEMENRISTEK-DIKTI) of the Republic of Indonesia through the World Class Professor Program (No. 168.A10/D2/KP/2017). The first author thanks Prof. Futoki Sakaida for providing A-HIGHERS data. A-HIGHERS data is the property of the Center for Atmospheric and Oceanic Studies, Tohoku University, Japan. The contact person for this data is Prof. Futoki Sakaida (email: toki@ocean.caos.tohoku.ac.jp). GPV data is available at http://gpvjma.ccs.hpcc.jp/~gpvjma/index.html.

References

Asai T (1996) Local meteorology. Todai Shuppankai, Tokyo

Chen G, Qin H (2016) Strong ocean-atmosphere interactions during a short-term hot event over the western Pacific warm pool in response to El Niño. J Climate 29(10):3841–3865. https://doi.org/10.1175/JCLI-D-15-0595.1

Clayson CA, Weitlich D (2006) Variability of tropical diurnal sea surface temperature. J Clim 20:334–352. https://doi.org/10.1175/JCLI3999.1

Franchito SH, Rao FB, Stech JL, Lorenzzetti JA (1998) The effect of coastal upwelling on the sea-breeze circulation at Cabo Frio, Brazil: a numerical experiment. Ann Geophys 16(7):866–881

Gentemann CL, Donlon CJ, Stuart-Menteeth A, Wentz FJ (2003) Diurnal signals in satellite sea surface temperature measurements. Geophys Res Lett 30(3):1140. https://doi.org/10.1029/2002GL016291

Katsaros KB (1980) The aqueous thermal boundary layer. Bound-Layer Meteorol 18:107–127

Kawai Y, Kawamura H (2002) Evaluation of the diurnal warming of sea surface temperature using satellite-derived marine meteorological data. J Oceanogr 58:805–814

Kawai Y, Wada A (2007) Diurnal sea surface temperature variation and its impact on the atmosphere and ocean: a review. J Oceanogr 63:721–744

Kawai Y, Otsuka K, Kawamura H (2006) Study on diurnal sea surface warming and a local atmospheric circulation over Mutsu Bay. J Meteorol Soc Jpn 84(4):725–744

Kawamura H, Wu P (1998) Formation mechanism of the Japan Sea proper water in the flux center off Vladivostok. J Geophys Res 103:611–622

Kawamura H, Qin H, Ando K (2008) In-situ diurnal sea surface temperature variations and near-surface thermal structure in the tropical Hot Event of the Indo-Pacific warm pool. J Oceanogr 64:847–857

Kim KR, Kim G, Kim K et al (2002) A sudden bottom water formation during the severe winter 2000–2001: the case of the East/Japan Sea. Geophys Res Lett 29(8):1234. https://doi.org/10.1029/2001GL014498

Morak-Bozzo S, Merchant CJ, Kent EC, Berry DI, Carella G (2016) Climatological diurnal variability in sea surface temperature characterized from drifting buoy data. Geosci Data J 3:20–28. https://doi.org/10.1002/gdj3.35

Nakayama I (1951) On the mean surface temperature of seas around Japan. In: Kobe B (ed) Mar Obs 159:1–16 **(in Japanese)**

Niino H (1987) The linear theory of land and sea breeze circulation. J Meteorol Soc Jpn 65:901–921

Park KA, Chung JY (1999) Spatial and temporal scale variations of sea surface temperature in the East Sea using NOAA/AVHRR data. J Oceanogr 55:271–288

Park KA, Lee EY (2014) Semiannual cycle of sea surface temperature in the East/Japan Sea and cooling process. Int J Remote Sens 35:4287–4314. https://doi.org/10.1080/01431161.2014.916437

Park KA, Chung JY, Kim K et al (2005) Wind and bathymetric forcing of the annual sea surface temperature signal in the East (Japan) sea. Geophys Res Lett 32:L5610. https://doi.org/10.1029/2004GL022197

Prytherch J, Farrar JT, Weller RA (2013) Moored surface buoy observations of the diurnal warm layer. J Geophys. Res. Oceans 118:4553–4569. https://doi.org/10.1002/jgrc.20360

Qin H, Kawamura H, Kawai Y (2007) Detection of hot event in the equatorial Indo-Pacific warm pool using advanced satellite sea surface temperature, solar radiation, and wind speed. J Geophys Res 112:C07015. https://doi.org/10.1029/2006JC003969

Robinson IS, Wells NC, Charnock H (1984) The sea surface thermal boundary layer and its relevance to the measurement of sea surface temperature by airborne and spaceborne radiometer. Int J Remote Sens 5:19–45

Saunders PM (1967) The temperature at the ocean-air interface. J Atmos Sci 24:269–273

Sakaida F, Kawamura H (1996) HIGHERS-the AVHRR-based higher spatial resolution sea surface temperature data set intended for studying the Ocean South of Japan. J Oceanogr 52:441–455

Sakaida F, Kudoh J, Kawamura H (2000) A-HIGHERS: the system to produce the high spatial resolution sea surface temperature maps of the North Pacific using the AVHRR/NOAA. J Oceanogr 56:707–716

Shimada T, Sawada M, Sha W, Kawamura H (2010) Low-level easterly winds blowing through the Tsugaru Strait, Japan. Part I: case study and statistical characteristic based on observations. Mon Weather Rev. https://doi.org/10.1175/2010MWR3354.1

Stull RB (1988) An introduction to boundary layer meteorology. Kluwer, Dordrecht, pp 257–258

Sverdrup HU, Johnson MW, Fleming RH (1942) The ocean: their physics, chemistry and general biology. Prentice-Hall, Englewood Cliffs, p 1087

Sweeney JK, Chagnoon JM, Gray JL (2014) A case study of sea breeze blocking regulated by sea surface temperature along the English south coast. Atmos Chem Phys 14:4409–4418. https://doi.org/10.5194/acp-14-4409-2014

Talley LD, Lobanov V, Ponomarev V et al (2003) Deep convection and brine rejection in the Japan Sea. Geophys Res Lett 30:1159. https://doi.org/10.1029/2002GL016451

Toyozumi T (2004) Study on coastal SST variation influenced by orographically steered surface wind, Master Thesis. Graduate School of Science, Tohoku University

Ward B, Donelan MA (2006) Thermometric measurements of the molecular sublayer at the air-water interface. Geophys Res Lett 33:L07605. https://doi.org/10.1029/2005GL024769

Webster PJ, Clayson CA, Curry JA (1996) Clouds, radiation, and the diurnal cycle of sea surface temperature in the tropical western Pacific. J Climate 9:1712–1730

Wirasatriya A, Kawamura H, Shimada T, Hosoda K (2015) Climatology of hot events in the western equatorial Pacific. J Oceanogr 71:77–90. https://doi.org/10.1007/s10872-014-0263-3

Wirasatriya A, Kawamura H, Shimada T, Hosoda K (2016) Atmospheric structure favoring high sea surface temperatures in the western equatorial Pacific. J Geophys Res Atmos 121:1–14. https://doi.org/10.1002/2016JD025268

Wirasatriya A, Setiawan RY, Subardjo P (2017) The effect of ENSO on the variability of chlorophyll-*a* and sea surface temperature in the Maluku Sea. IEEE J Stars 10(12):5513–5518. https://doi.org/10.1109/JSTARS.2017.2745207

Yamaguchi S, Kawamura H (2005) Influence of orographycally steered winds on Mutsu Bay surface currents. J Geophys Res 110:C09010. https://doi.org/10.1029/2004JC002462

Zeng X, Dickinson RE (1998) Impact of diurnally-varying skin temperature on surface fluxes over the tropical Pacific. Geophys Res Lett 25:1411–1414

Satellite-borne detection of high diurnal amplitude of sea surface temperature in the seas west of the Tsugaru Strait, Japan, during Yamase wind season

GRADEMARK REPORT

FINAL GRADE

/0

GENERAL COMMENTS

Instructor

PAGE 1

PAGE 2

PAGE 3

PAGE 4

PAGE 5

PAGE 6

PAGE 7

PAGE 8

PAGE 9

PAGE 10

PAGE 11

PAGE 12

PAGE 13

PAGE 14